NUCLEAR SCIENCE AND ENGINEERING: **153**, 8–25 (2006)

Neutron Transmission and Capture Measurements and Resonance Parameter Analysis of Neodymium from 1 to 500 eV

D. P. Barry,*† M. J. Trbovich, Y. Danon, R. C. Block, and R. E. Slovacek

Rensselaer Polytechnic Institute, Mechanical, Aerospace and Nuclear Engineering Department
Troy, New York 12180-3590

and

G. Leinweber, J. A. Burke, and N. J. Drindak

KAPL Inc., Lockheed Martin Corporation, P.O. Box 1072, Schenectady, New York 12301-1072

Received February 18, 2005
Accepted September 7, 2005

Abstract—*Neodymium is a ^{235}U fission product and is important for reactor neutronic calculations. The aim of the present work is to improve upon the existing neutron cross-section data of neodymium.*

Neutron capture and transmission measurements were performed by the time-of-flight technique at the Rensselaer Polytechnic Institute (RPI) linear accelerator (LINAC) laboratory using metallic neodymium samples. The capture measurements were made at the 25-m flight station with a 16-segment NaI multiplicity detector, and the transmission measurements were performed at 15- and 25-m flight stations, respectively, with ^{6}Li glass scintillation detectors. After the data were collected and reduced, resonance parameters were determined by combined fitting of the transmission and capture data with the SAMMY multilevel R-matrix Bayesian code.

The resonance parameters for all naturally occurring neodymium isotopes were deduced within the energy range of 1 to 500 eV. The resulting resonance parameters were used to calculate the capture resonance integrals from this energy. The RPI parameters gave a resonance integral value of 32 ± 1 b that is ~7% lower than that obtained with the ENDF/B-VI parameters. The current measurements significantly reduce the uncertainties of the resonance parameters when compared with previously published parameters.

I. INTRODUCTION

To improve the accuracy of neodymium cross-section data, the Rensselaer Polytechnic Institute (RPI) Cross-Section Group has performed neutron time-of-flight (TOF) measurements using elemental neodymium samples at the RPI linear accelerator (LINAC) facility. Transmission and capture measurements were performed, and the resulting data were analyzed in a combined method with the SAMMY R-matrix Bayesian fitting code[1] to determine resonance parameters.

The RPI Cross-Section Group has made extensive efforts to improve the experimental equipment used in the measurements. A 16-segment NaI multiplicity detector has been developed for use in neutron capture measurements.[2] An improved TOF analyzer was designed and constructed with the ability to handle high counting rates while providing good accuracy.[3] Improvements have also been made on LINAC neutron-production targets at energies of interest.[4–6] Additionally, data reduction software has been written to manipulate the data.

II. EXPERIMENTAL CONDITIONS

The RPI LINAC facility uses a 60-MeV pulsed electron beam to produce neutrons by means of photonuclear

*E-mail: barrydp@kapl.gov
†Current address: KAPL Inc., Lockheed Martin Corporation, P.O. Box 1072, Schenectady, New York 12301-1072

reactions. The electron beam impinges upon a water-cooled tantalum target where electrons interact and produce bremsstrahlung radiation, which in turn generates photoneutrons. The resulting neutrons are moderated and collimated as they travel through a long evacuated flight tube to the sample and detector.

The present RPI neodymium data were obtained from four sets of measurements performed at the RPI LINAC facility. Two of the measurements were transmission, and two were neutron capture. The details of each experiment are given in Table I.

Two different neutron-production targets were used in the present series of neodymium measurements. The bare-bounce target[4] (BBT) was employed for epithermal transmission and capture measurements. The BBT geometry is unique in that the tantalum plates are mounted off the neutron beam axis. A 2.54-cm-thick polyethylene moderator is mounted adjacent to the tantalum plates and centered on the neutron beam axis. The moderator effectively slows down the fast neutrons generated in the target through collisions with hydrogen and emits the neutrons at a lower energy. These moderated neutrons then drift down an evacuated flight tube to the detector. The epithermal measurements also incorporate a 0.8-cm-thick B_4C overlap filter placed in-beam to remove low-energy neutrons from previous pulses.

The enhanced thermal target[5] (ETT) was utilized in the thermal transmission and capture measurements. The ETT was designed to produce high neutron flux for use in thermal measurements. This target consists of water-cooled tantalum plates, a water moderator, a polyethylene moderator on the neutron beam axis, and a graphite reflector.

The TOF technique was used to determine the neutron energy for each detected event. The time that it takes for a neutron to travel a known flight path distance to the neutron detector defines the energy of the neutron. The TOF analyzer[3] used in these experiments utilizes a 32-MHz crystal oscillator coupled to a high-speed scaler with 22-bit resolution. The TOF analyzer has a fixed dead time of 0.250 μs to record each detected event. The overall dead time of the signal-processing electronics was set to 0.6 μs for transmission experiments and 1.125 μs for capture experiments. A Hewlett-Packard HP-1000 Model A990 computer was used to record the data and control the sample changer. The sample changer can hold up to eight samples and rotate them in and out of the neutron beam.

Table II lists all the samples used in each of the RPI neodymium experiments. The samples were composed of natural neodymium metal (99.9% purity) and sealed inside of an aluminum sample can. There were considerable impurities in the samples, most notably the strong thermal absorber gadolinium. It was, therefore, impractical to use the neodymium samples to extract thermal data. The impurities, however, have negligible impact at epithermal energies above ~1 eV. The thickness of aluminum on the front and back surface of each sample was 0.51 mm. The additional thickness of aluminum in the sample can was taken into account by including empty sample cans in the measurements. The amount of time each sample was placed in the neutron beam was optimized to minimize experimental errors in the counting statistics. The sample characteristics are found in Table III. The mass of each individual sample was determined using a Fisher Scientific chain balance with an accuracy of 0.1 mg.

II.A. Transmission Detectors

Neutron transmission experiments were performed at the 15- and 25-m flight stations at the RPI LINAC facility. Thermal transmission experiments were conducted at the 15-m station, which contains a 7.62-cm

TABLE I

Neodymium Experimental Details

Experiment	Neutron-Producing Target	Electron Pulse Width (ns)	Channel Width (μs)	Channel Width Energy Range	Pulse Repetition Rate (pulse/s)	Flight Station (m)
Epithermal transmission	BBT	52	0.25 0.125	2.7 to 53 eV >53 eV	250	25
Thermal transmission	ETT	290	0.5 0.25	0.5 to 3.2 eV >3.2 eV	25	15
Epithermal capture	BBT	56	0.25 0.125	2.7 to 53 eV >53 eV	200	25
Thermal capture	ETT	1000	0.5 0.25	0.5 to 3.2 eV >3.2 eV	25	25

TABLE II

Neodymium Samples Used

Nominal Sample Thickness			Experiment			
(cm)	(in.)	(mils)	Epithermal Transmission	Thermal Transmission	Epithermal Capture	Thermal Capture
0.005	0.002	2			X	X
0.013	0.005	5			X	X
0.025	0.010	10			X	X
0.051	0.020	20	X			X
0.089	0.035	35	X	X		
0.127	0.050	50	X	X		
0.254	0.100	100	X	X		
0.508	0.200	200	X	X	X	X
1.016	0.400	400	X	X		

(3-in.)-diam, 0.3-cm-thick in-beam NE 905 ^{6}Li loaded scintillator glass (6.6% lithium, enriched in ^{6}Li to 95%). This thermal transmission detector is used for measurements within the energy range of 0.001 to 20 eV. The epithermal transmission measurements were performed at the 25-m station, which housed a 12.7-cm (5-in.)-diam, 1.27-cm-thick (0.5-in.) in-beam Bicron GS-20 ^{6}Li loaded scintillator glass (6.6% lithium, enriched in ^{6}Li to 95%). The epithermal transmission detector is used to cover the energy range from 1 to 500 eV.

Each of the transmission detectors is coupled to a single photomultiplier tube, which is placed in line with the flight path. The flight path distance for the epithermal transmission detector was 25.597 m from the BBT, while the flight path for the thermal transmission measurements was 14.973 m from the ETT.

The metallic neodymium samples, along with empty sample cans, were mounted on an eight-position sample changer that was computer controlled during the transmission experiments. The transmission was determined by finding the ratio of the background-corrected sample-in count rate to the background-corrected sample-out count rate. Each LINAC run consisted of a complete cycle through all samples on the changer. The amount of time each sample was placed in-beam was optimized to minimize the counting statistics error in the measurement.

II.B. Capture Detector

The RPI capture detector[2] is a 30.5-cm-diam × 30.5-cm-high (12- × 12-in.) hollow cylinder that contains 16 sections of thallium activated sodium iodide NaI(Tl)

TABLE III

Neodymium Sample Characteristics

Nominal Sample Thickness			Sample Weight (g)	Weight Error (g)	Average Diameter (in.)	Diameter Error (in.)	Number Density (atom/b)	Number Density Fractional Error
(cm)	(in.)	(mils)						
0.005	0.002	2	0.6165	0.0001	1.987	0.002	0.0001287	0.002020
0.013	0.005	5	1.7908	0.0001	1.983	0.001	0.0003751	0.001010
0.025	0.010	10	3.4111	0.0001	1.981	0.001	0.0007164	0.001010
0.051	0.020	20	6.8575	0.0001	1.981	0.001	0.001440	0.001010
0.089	0.035	35	12.5393	0.0001	1.976	0.002	0.002646	0.002024
0.127	0.050	50	18.4885	0.0001	1.984	0.001	0.003870	0.001008
0.254	0.100	100	34.6764	0.0001	1.983	0.002	0.007267	0.002017
0.508	0.200	200	67.3220	0.0001	1.982	0.002	0.01411	0.002018
1.016	0.400	400	141.8704	0.0001	1.982	0.002	0.02975	0.002018

scintillator crystals. The cylinder is split perpendicular to its axis into two rings, and each ring contains eight equally sized pie-shaped NaI(Tl) segments. Each NaI(Tl) segment is optically isolated and hermetically sealed within an aluminum can and mounted on an RCA 8575 photomultiplier. The total volume of NaI(Tl) within the detector is 20 ℓ. The incident neutron beam is collimated and directed through an 8.9-cm (3.5-in.) cylindrical through-hole in the detector where it impinges upon a sample placed in the center. An annular boron carbide liner (enriched in ^{10}B) separates the NaI(Tl) crystals from the sample. The boron liner absorbs neutrons that are scattered from the sample and prevents them from reaching the NaI(Tl) crystal, thus reducing any scattering background contribution. The detector is surrounded by a 15-cm (6-in.)-thick, 7260-kg (16 000-lb) lead shield to reduce ambient background signals. The capture detector is located at a flight path distance of 25.56 m from the BBT during epithermal capture measurements and 25.41 m from the ETT during thermal capture measurements. The efficiency of the capture detector is assumed to be the same for all neodymium isotopes.

The metallic neodymium samples were accurately positioned in the center of the RPI capture detector by a sample changer. The sample changer has eight positions and is computer controlled during the capture experiments. Each LINAC run consisted of a complete cycle through all samples on the changer. The amount of time each sample was placed in-beam was optimized to minimize the counting statistics error in the measurement.

III. DATA REDUCTION

III.A. Transmission Data

The RPI LINAC electron beam pulse width and TOF channel widths for the Nd experiments are listed in Table I. The average LINAC current on the BBT for the epithermal transmission measurements was ~30 μA. The average LINAC current on the ETT for the thermal measurements was ~4.5 μA. Each of these transmission runs lasted ~60 h (Ref. 7).

A TOF spectrum with 8192 channels was collected for each sample used in the transmission measurement. This large amount of TOF data collected in each measurement was initially run through a statistical integrity check. The integrity check verified the stability of the RPI LINAC, the transmission detector, and associated beam monitors. The data were accepted only if the detector and beam monitor counts fell within an acceptable range of statistical fluctuations. This check identified LINAC malfunctions and other problems in the system that would cause loss of counts. All data that did not pass the integrity test were eliminated. The data were then corrected for dead time, and runs were normalized to beam monitors and summed. Time-dependent background measurements were obtained with the notch-one, notch-two method.[8] This background method utilizes blacked-out notch filters consisting of single (notch-1) and double (notch-2) material thicknesses. The resulting background determined from each notch filter was extrapolated to a zero effective material thickness. The measured background was then fitted to a smooth analytical function of TOF that was used for the time-dependent background correction. The calculation of the transmission in TOF channel i was calculated by

$$T_i = \frac{C_i^s - K_s B_i - B_s}{C_i^o - K_o B_i - B_o} \quad , \tag{1}$$

where

C_i^s, C_o^s = dead-time corrected and normalized count rates of the sample and open measurements, respectively

B_i = time-dependent background count rate

B_s, B_o = steady-state background count rates for the sample and open measurements, respectively

K_s, K_o = normalization factors for the sample and open measurements, respectively.

For epithermal transmission measurements, the normalization factors for each sample were found by forcing the average transmission to zero in the blackout region of the strong 42-eV neodymium resonance. In the thermal transmission measurements, the normalization factors for each sample were found by forcing the average transmission to zero in the blackout region of a saturated 1.46-eV indium fixed-notch resonance.

III.B. Capture Data

The capture experiments performed at the RPI LINAC facility require taking several types of data. The sample data were taken with up to eight samples placed on the sample changer. Four of the samples were metallic neodymium of varying thicknesses. Sixteen TOF multiplicity spectra with 8192 channels were measured for each sample. A minimum energy threshold of 100-keV deposited gamma-ray energy was required for a detector segment to be counted. Data were recorded as capture events only if the total energy deposited in all 16 segments was $>$1 MeV. The data were recorded as scattering events if the total deposited gamma-ray energy fell within the energy range of 360 to 600 keV. This scattering energy region contains the 478-keV gamma ray emitted from the $(n;\alpha,\gamma)$ reaction that occurs when scattered neutrons are absorbed in the $^{10}B_4C$ detector liner.

The RPI LINAC electron beam pulse width and TOF channel widths for the Nd capture experiments are listed in Table I. The average LINAC current on the BBT for the epithermal transmission measurements was ~30 μA.

The average LINAC current on the ETT for the thermal measurements was ~5.6 μA. Each capture measurement lasted ~60 h (Ref. 7).

As with the transmission measurements, the large amount of TOF data collected in each capture measurement was subjected to statistical integrity checks, as discussed previously, to verify the stability of the LINAC, the capture detector, and associated beam monitors. Any data that failed the integrity test were eliminated. Next, the data were dead-time corrected, normalized to beam monitors, and summed. The background was determined using normalized data measured with an empty aluminum can mounted on the sample changer. This background was subtracted from the normalized and summed capture spectra. The 16 individual capture spectrums were then summed into a single total spectrum.

The TOF capture data are presented in terms of capture yield. The capture yield in TOF channel i was calculated by

$$Y_i = \frac{C_i - B_i}{K\phi_i} \quad , \tag{2}$$

where

C_i = dead-time corrected and monitor-normalized count rate of the sample measurement

B_i = monitor-normalized background counting rate

K = detector efficiency and flux normalization factor

ϕ_i = monitor-normalized incident neutron flux shape.

The incident neutron flux shape was determined with the use of a thick $^{10}B_4C$ sample (enriched to 98.11% ^{10}B) that is mounted on the sample changer. During this flux measurement, the total energy threshold of the detector was adjusted to record the 478-keV gamma rays resulting from neutron absorption in ^{10}B. A B_4C sample is used since it effectively absorbs all the incident neutrons over the energy range of interest. The measurement is corrected for the transmission through the B_4C sample. This boron capture spectrum provides an accurate determination of the incident neutron flux shape.

The measured flux shape is usually normalized directly to a saturated capture resonance. However, this was not possible in this experiment because there were no saturating resonances found in the neodymium capture data. For this reason, SAMMY was used to find the appropriate capture normalization. The first step was to fit the thermal transmission data at 4 eV and obtain resonance parameters. The second step was to hold these resonances constant while performing a combined thermal transmission and capture fit at 4 eV while fitting normalization. The resulting normalized thermal capture yield data were then used to cross normalize the epithermal data at the 42-eV neodymium capture resonance. The 42-eV neodymium resonance was chosen for normalization of the epithermal capture data because it had good statistics.

IV. METHODS

Resonance parameters were extracted from the Nd transmission and capture data sets using the SAMMY multilevel R-matrix Bayesian code.[1] The SAMMY code enabled a combined transmission and capture analysis, while employing multiple scattering, self-shielding, and resolution-broadening features. The resolution broadening describes the cumulative effect of the RPI LINAC electron burst width, the moderator slowing-down time, the TOF channel width, and the effect of the detector. The electron burst width and the TOF channel width are entered as SAMMY input parameters. All remaining resolution function components are described by an analytical function of magnitude versus time whose integral over time is unity.

A key factor in fitting the correct shape to the experimental data is knowledge of the resolution function, which has a significant impact on the shape analysis fitting process, especially at epithermal energies. It can be stated with confidence that inaccuracy in the shape of the resolution function can translate into imprecise resonance parameters when fitting experimental data. For this reason, the epithermal transmission and capture resolution functions were fit to well-known ^{238}U resonances using SAMMY. Special attention was given to epithermal energy regions since the resolution function has greater influence in this energy region, as compared to thermal energy. The RPI resolution function was used for the transmission measurements, while a Gaussian plus exponential tail function was used for the capture measurements. Both of these resolution functions are explicit options within SAMMY.

As a starting point, the SAMMY fits utilized Nd parameters from the ENDF/B-VI evaluation.[9] The spins and isotopic assignments for every observed resonance were taken from ENDF/B-VI and were not changed. Additionally, the potential scattering radius for each isotope was fixed at the ENDF/B-VI values. It should be noted that ENDF/B-VI does not include uncertainties of the potential scattering radius values. The evaluation in Mughabghab, Divadeenam, and Holden[10] does include these uncertainties, but they were not included in our analysis. Based on sensitivity studies, it is estimated that errors in the resonance parameters resulting from errors in the scattering radius are below the errors reported in this paper. The thermal data were used to extract parameters for the 4.35-eV resonance only. A combined transmission and capture fit was performed over the energy range of 4.0 to 4.8 eV. The experimental transmission data used in the fitting process were from the 0.051-cm (0.02-in.), 0.089-cm (0.035-in.), 0.127-cm (0.05-in.), and

0.0254-cm (0.1-in.) samples. The background shape was inaccurate for the thick 0.508-cm (0.2-in.) and 1.016-cm (0.4-in.) samples, presumably the result of local flux depression. The 0.508-cm (0.2-in.) and 1.016-cm (0.4-in.) data were, therefore, removed from the SAMMY analysis to improve the overall accuracy in the fit to this resonance. The capture data that were used in the SAMMY analysis were those from the 0.013-cm (0.005-in.), 0.025-cm (0.01-in.), and 0.051-cm (0.02-in.) samples. The 0.005-cm (0.002-in.) capture data were not used in the fitting procedure since the yields were extremely small and contributed little to the overall SAMMY fit. The thermal transmission and capture data were fed into SAMMY using a serial routine where the covariance and parameter outputs from one particular sample run were used as input for the next sample to be fit. Only the relevant resonance parameters E, Γ_n, and Γ_γ were allowed to vary.

The epithermal resonance data, for both transmission and capture, were examined over the energy range of 30 to 500 eV. Once again, the Nd parameters from the ENDF/B-VI evaluations were used as the starting-point values. The transmission and capture data were input into SAMMY using the same serial routine as used in the thermal analysis. When fitting with SAMMY it was observed that the shape of the thick samples could not be fitted accurately at the 42-eV resonance. This was attributed to a local flux depression caused by the large strength of this resonance that removes neutrons from the beam. It was, therefore, decided to exclude the 0.254-cm (0.1-in.), 0.508-cm (0.2-in.), and 1.016-cm (0.4-in.) experimental data below 50 eV during the fitting process.

The errors on the final SAMMY resonance parameters are purely statistical errors that do not account for certain experimental uncertainties, such as those arising from the experimental resolution function. It is necessary to estimate the impact of the resolution function uncertainty upon the final Nd parameters extracted from SAMMY. The sensitivity of the resolution function to changes in its parameters was investigated with the same uranium data used for fitting the resolution function. That study determined the value of the resolution function parameters that caused a $\pm 10\%$ change in the reduced chi-square value, relative to the optimum value (i.e., best fit). It should be noted that a change of 10% in chi-square corresponds to the fit moving $\sim\frac{1}{20}$ of a standard deviation from the best fit. The values of the resolution function parameters that caused a $\pm 10\%$ change in reduced chi-square were considered to be the "estimated uncertainty" in that parameter. To see the impact on the final Nd resonance parameters, the transmission and capture resolution function parameters were changed to these estimated uncertainty values. The combined SAMMY fits in thermal and epithermal neodymium were then repeated incorporating these uncertainty values. It should be emphasized that only one resolution function parameter was changed at a time, while all the other parameters were kept at the optimum value. These uncertainty resonance parameters were then compared to the final Nd parameters found with use of the optimal resolution function. This comparison allowed for the estimation of the error of the final resonance parameters due to the uncertainties in the resolution function as shown in Tables IV and V.

V. RESULTS AND DISCUSSION

The final RPI neodymium parameters resulting from the combined SAMMY fits are presented in Table IV along with evaluated parameters from ENDF/B-VI (Ref. 9) and Mughabghab, Divadeenam, and Holden.[10] ENDF/B-VI uses Mughabghab, Divadeenam, and Holden resonance parameters for the ^{144}Nd, ^{146}Nd, ^{148}Nd, and ^{150}Nd isotopes. All unknown resonance spins given by Mughabghab, Divadeenam, and Holden were assumed to be the same spin as those listed in ENDF/B-VI. This allowed the conversion of $2g\Gamma_n$ values presented by Mughabghab, Divadeenam, and Holden to Γ_n. The errors from the SAMMY fits are shown under the RPI parameter values in parentheses, while estimated errors due to the RPI resolution function are placed in square brackets. The RPI parameters were rounded to the larger of these two error values. The radiation width for the 96.15-eV resonance (in ^{145}Nd) was fixed at an average value since SAMMY could not provide an adequate fit because of insensitivity. The error in this average was taken to be the standard deviation determined for this average.

Examples of the combined SAMMY fits using the final RPI neodymium parameters (Table IV) are presented in Figs. 1 through 6. Figures 1 and 2 show high-quality fits to the resonance at 4.35 eV for transmission and capture yield, respectively. Figures 3 and 4 show excellent fits to the resonance at 42.55 eV for both transmission and capture yield. Figures 5 and 6 exemplify the complexity of the neodymium data in the energy region from 300 to 440 eV. In this energy region there are many resonances that can influence each other; the most influential is the massive ^{144}Nd resonance at 374.4 eV. Figure 6 shows that SAMMY gives good fits even with large multiple scattering effects, with the exception of the 390.98-eV resonance, which seems to be off by a factor of ~ 2.

The ENDF/B-VI resonance parameters for ^{143}Nd and ^{145}Nd isotopes are based upon the work of Tellier[11,12] and Rohr, Weigmann, and Heske.[13] For this reason, the RPI parameters are listed again in Table V with the experimental parameters from Tellier and Rohr, Weigmann, and Heske. Tellier presented Γ_t and $2g\Gamma_n$ values for each neodymium resonance. In very few instances the $2g\Gamma_\gamma$ values were also listed, leading to the conclusion that Tellier could not offer much information about the radiation width. All unknown resonance spins in the

TABLE IV

Final RPI Resonance Parameters Along with the Evaluations of ENDF/B-VI and Mughabghab, Divadeenam, and Holden*

RPI			ENDF/B-VI			Mughabghab, Divadeenam, and Holden			
E (eV)	Γ_γ (meV)	Γ_n (meV)	E (eV)	Γ_γ (meV)	Γ_n (meV)	E (eV)	Γ_γ (meV)	Γ_n (meV)	Isotope and Spin
^{143}Nd									
55.390 (0.001) [0.004]	68 (1) [0.4]	37.7 (0.2) [0.1]	55.33	75	36.71	55.33 (0.05)	75 (10)	36.7 (1)	143 $I = 7/2$ $J = 4$
127.49 (0.002) [0.01]	88 (1) [0.1]	411.7 (1) [0.2]	127.40	70	388.57	127.4 (0.1)	70 (10)	389 (23)	143 $I = 7/2$ $J = 3$
135.60 (0.002) [0.01]	76 (2) [2]	57.9 (0.5) [0.3]	135.50	65	64.00	135.5 (0.1)	65 (14)	64 (6)	143 $I = 7/2$ $J = 3$
159.04 (0.004) [0.02]	63 (1) [0.4]	977 (4) [2]	158.90	76	977.78	158.9 (0.1)	76 (3)	977.8 (71)	143 $I = 7/2$ $J = 4$
179.71 (0.003) [0.02]	76 (1) [0.2]	733 (2) [0.4]	179.50	74	657.14	179.5 (0.2)	74 (5)	657 (29)	143 $I = 7/2$ $J = 3$
186.80 (0.003) [0.02]	67 (1) [0.08]	1403 (3) [0.4]	186.60	76	1377.78	186.6 (0.2)	76 (3)	1378 (88.9)	143 $I = 7/2$ $J = 4$
306.51 (0.007) [0.06]	69 (2) [6]	773 (4) [5]	306.20	72	684.44	306.2 (0.3)	72 (5)	684 (36)	143 $I = 7/2$ $J = 4$
324.77 (0.008) [0.06]	70 (2) [1]	1041 (6) [3]	324.40	59	934.86	324.4 (0.3)	59 (7)	935 (46)	143 $I = 7/2$ $J = 3$
337.49 (0.009) [0.05]	66 (2) [0.2]	789 (7) [3]	337.20	57	666.67	337.2 (0.3)	57 (4)	667 (53)	143 $I = 7/2$ $J = 4$
350.71 (0.02) [0.05]	87 (3) [0.3]	1010 (14) [7]	350.40	85	880.00	350.4 (0.3)	85 (5)	880 (46)	143 $I = 7/2$ $J = 3$
401.93 (0.002) [0.07]	67 (3) [2]	1050 (21) [10]	401.30	77	967.11	401.3 (0.4)	81 (4)	967.1 (53)	143 $I = 7/2$ $J = 4$
408.49 (0.002) [0.06]	82 (3) [1]	630 (14) [21]	408.00	73	571.43	408 (0.4)	69 (4)	571 (34)	143 $I = 7/2$ $J = 3$
446.5 (0.001) [0.1]	82 (3) [2]	1787 (9) [4]	446.30	75	1742.22	446.3 (0.4)	80 (5)	1742 (44)	143 $I = 7/2$ $J = 4$
^{144}Nd									
374.40 (0.002) [0.06]	108 (1) [3]	16 730 (13) [18]	373.80	80	16 250.0	373.8 (0.4)	—	16 300 (500)	144 $I = 0$ $J = 1/2$

(Continued)

TABLE IV (Continued)

RPI			ENDF/B-VI			Mughabghab, Divadeenam, and Holden			
E (eV)	Γ_γ (meV)	Γ_n (meV)	E (eV)	Γ_γ (meV)	Γ_n (meV)	E (eV)	Γ_γ (meV)	Γ_n (meV)	Isotope and Spin
^{145}Nd									
4.36 (0.0002) [0.002]	69.6 (0.4) [0.1]	1.18 (0.003) [0.003]	4.35	51	1.37	4.35 (0.02)	51 (5)	1.37 (0.1)	145 $I = 7/2$ $J = 3$
—	—	—	18.9	65	0.00364	—	—	—	
42.55 (0.0008) [0.004]	64.9 (0.4) [0.05]	372.1 (0.7) [0.08]	42.51	57	354.29	42.51 (0.05)	57 (2)	354 (17)	145 $I = 7/2$ $J = 3$
85.73 (0.003) [0.007]	51 (3) [4]	11.8 (0.1) [0.03]	85.62	75	10.93	85.62 (0.08)	—	10.9 (0.8)	145 $I = 7/2$ $J = 3$
96.15 (0.006) [0.007]	60 (12)	6.6 (0.1) [0.03]	96.00	74	5.83	96 (0.1)	74 (10)	5.8 (0.2)	145 $I = 7/2$ $J = 4$
102.08 (0.001) [0.009]	69 (1) [0.4]	133.5 (0.7) [0.2]	101.95	47	131.43	102.95 (0.1)	47 (5)	131 (6)	145 $I = 7/2$ $J = 3$
103.60 (0.002) [0.009]	66 (3) [1]	32.6 (0.3) [0.1]	103.45	65	34.67	103.45 (0.1)	65 (10)	35 (1.1)	145 $I = 7/2$ $J = 3$
147.30 (0.005) [0.01]	42 (3) [8]	21.8 (0.3) [0.5]	147.10	75	18.67	147.1 (0.2)	—	19 (1.3)	145 $I = 7/2$ $J = 4$
151.62 (0.009) [0.01]	64 (5) [2]	13.7 (0.4) [0.3]	151.40	75	13.07	151.4 (0.2)	—	13.1 (0.2)	145 $I = 7/2$ $J = 4$
169.94 (0.03) [0.01]	60 (6) [2]	4.4 (0.2) [0.04]	169.70	75	2.67	169.7 (0.2)	—	3 (0.2)	145 $J = 4$
189.45 (0.01) [0.01]	82 (6) [4]	36 (1) [0.4]	189.20	38	37.71	189.2 (0.2)	38 (3)	38 (2)	145 $I = 7/2$ $J = 3$
233.00 (0.03) [0.1]	57 (6) [3]	6.3 (0.4) [0.4]	232.60	75	5.87	232.6 (0.2)	—	5.9 (0.4)	145 $J = 4$
242.53 (0.009) [0.03]	48 (2) [1]	62 (1) [0.7]	242.10	51	62.22	242.1 (0.2)	51 (4)	62 (3)	145 $I = 7/2$ $J = 4$
248.70 (0.03) [0.4]	57 (6) [2]	5.0 (0.4) [0.2]	248.40	75	4.34	248.4 (0.2)	—	4.3 (0.5)	145 $J = 3$
259.25 (0.008) [0.03]	55 (2) [2]	82 (1) [1]	258.90	44	88.89	258.9 (0.2)	44 (3)	88.9 (4)	145 $I = 7/2$ $J = 4$
275.19 (0.008) [0.04]	53 (2) [1]	142 (2) [2]	274.80	48	130.67	274.8 (0.2)	48 (3)	131 (7)	145 $J = 4$

(Continued)

TABLE IV (Continued)

RPI			ENDF/B-VI			Mughabghab, Divadeenam, and Holden			
E (eV)	Γ_γ (meV)	Γ_n (meV)	E (eV)	Γ_γ (meV)	Γ_n (meV)	E (eV)	Γ_γ (meV)	Γ_n (meV)	Isotope and Spin
^{145}Nd (Continued)									
306.71 (0.06) [0.3]	33 (3) [2]	50 (5) [10]	306.20	35	66.29	306.2 (0.3)	35 (5)	66 (14)	145 $I = 7/2$ $J = 3$
311.54 (0.01) [0.05]	61 (2) [0.8]	418 (7) [4]	311.10	39	346.29	311.1 (0.3)	39 (4)	346 (17)	145 $I = 7/2$ $J = 3$
318.78 (0.03) [0.5]	61 (6) [3]	10.5 (0.8) [0.8]	318.50	75	10.67	318.5 (0.3)	—	11 (1)	145 $I = 7/2$ $J = 4$
342.89 (0.01) [0.09]	70 (6) [12]	51 (3) [1]	342.50	75	51.56	342.5 (0.3)	—	52 (3)	145 $I = 7/2$ $J = 4$
376.14 (0.02) [0.4]	59 (6) [2]	10 (1) [2]	376.60	75	9.96	376.6 (0.3)	—	9.96 (0.5)	145 $I = 7/2$ $J = 4$
390.98 (0.08) [0.07]	40 (3) [23]	50 (4) [24]	390.50	25.4	40.89	390.5 (0.4)	25.4 (3.4)	41 (7)	145 $I = 7/2$ $J = 4$
397.80 (0.1) [0.5]	74 (7) [0.5]	28 (3) [2]	397.70	75	30.86	397.7 (0.4)	—	31 (2)	145 $I = 7/2$ $J = 3$
404.21 (0.04) [0.07]	61 (4) [4]	230 (15) [36]	403.60	75	195.56	403.6 (0.4)	—	196 (18)	145 $I = 7/2$ $J = 4$
406.49 (0.05) [0.1]	50 (4) [12]	120 (9) [19]	406.20	75	115.56	406.2 (0.4)	—	116 (4)	145 $I = 7/2$ $J = 4$
446.58 (0.08) [0.1]	52 (5) [2]	150 (14) [16]	445.80	58	228.57	445.8 (0.4)	58 (5)	229 (23)	145 $I = 7/2$ $J = 3$
465.16 (0.02) [0.1]	82 (4) [1]	800 (10) [5]	464.60	58	748.57	464.6 (0.5)	58 (5)	749 (40)	145 $I = 7/2$ $J = 3$
487.59 (0.05) [0.1]	65 (4) [5]	230 (19) [15]	487.10	75	315.56	487.1 (0.5)	58 (5)	316 (13)	145 $I = 7/2$ $J = 4$
497.87 (0.02) [0.1]	68 (4) [0.06]	455 (9) [8]	497.20	63	457.14	497.2 (0.5)	63 (5)	457 (23)	145 $I = 7/2$ $J = 3$
^{146}Nd									
359.9 (0.007) [0.1]	35 (2) [9]	50 (3) [17]	359.50	55	44	359.5 (0.3)	—	44 (3)	146 $I = 0$ $J = 1/2$
(Continued)									

TABLE IV (Continued)

RPI			ENDF/B-VI			Mughabghab, Divadeenam, and Holden			
E (eV)	Γ_γ (meV)	Γ_n (meV)	E (eV)	Γ_γ (meV)	Γ_n (meV)	E (eV)	Γ_γ (meV)	Γ_n (meV)	Isotope and Spin
^{148}Nd									
94.93 (0.04) [0.02]	46 (5) [2]	0.55 (0.04) [0.01]	94.90	67	0.53	94.9 (0.1)	—	0.53 (0.05)	148 $I = 0$ $J = 1/2$
155.59 (0.004) [0.02]	41.8 (0.8) [0.4]	2034 (5) [2]	155.40	70	1650	155.4 (0.1)	70 (8)	1650 (200)	148 $I = 0$ $J = 1/2$
172.4 (0.1) [0.01]	45 (5) [0.2]	0.45 (0.04) [0.07]	172.40	67	0.41	172.4 (0.2)	—	0.41 (0.03)	148 $I = 0$ $J = 1/2$
184.4 (0.2) [0.08]	45 (5) [0.02]	0.071 (0.007) [0.001]	—	—	—	184.5 (0.2)	—	0.07 (0.05)	148 $J = 1/2$
252.9 (0.2) [0.4]	45 (5) [0.1]	0.38 (0.004) [0.02]	252.90	67	0.40	252.9 (0.2)	—	0.4 (0.1)	148 $I = 0$ $J = 1/2$
287.66 (0.006) [0.04]	35 (1) [0.2]	3043 (6) [3]	287.50	58	3160.00	287.5 (0.3)	58 (6)	3160 (200)	148 $I = 0$ $J = 1/2$
398.84 (0.03) [0.08]	59 (3) [3]	340 (14) [7]	398.30	65	380.00	398.3 (0.4)	65 (10)	380 (30)	148 $I = 0$ $J = 1/2$
^{150}Nd									
78.92 (0.002) [0.007]	45 (2) [6]	17.3 (0.1) [0.1]	78.80	52	18.4	78.8 (0.1)	52 (10)	18.4 (0.5)	150 $I = 0$ $J = 1/2$
265.9 (0.3) [0.06]	52 (5) [0.01]	0.39 (0.04) [0.02]	265.90	72	0.4	265.9 (0.2)	—	0.4 (0.05)	150 $I = 0$ $J = 1/2$
313.62 (0.01) [0.05]	55 (2) [1]	402 (6) [4]	313.20	66	425	313.2 (0.3)	66 (10)	425 (15)	150 $I = 0$ $J = 1/2$
458.9 (0.1) [0.6]	52 (5) [0.1]	1.5 (0.1) [0.02]	459.00	72	1.50	459 (0.5)	—	1.5 (0.25)	150 $I = 0$ $J = 1/2$
486.4 (0.02) [0.1]	56 (3) [3]	1030 (18) [9]	486.00	74	1000.00	486 (0.5)	74 (11)	1000 (50)	150 $I = 0$ $J = 1/2$

*The RPI parameters have errors from SAMMY fits in parentheses ( ) and errors from the resolution function in square brackets [ ]. The errors from Mughabghab, Divadeenam, and Holden are presented in parentheses.

TABLE V

Final RPI Resonance Parameters Along with Experimental Tellier and Rohr, Weigmann, and Heske Parameters*

RPI			Tellier			Rohr, Weigmann, and Heske			
E (eV)	Γ_γ (meV)	Γ_n (meV)	E (eV)	Γ_γ (meV)	Γ_n (meV)	E (eV)	Γ_γ (meV)	Γ_n (meV)	Isotope and Spin
^{143}Nd									
55.390 (0.001) [0.004]	68 (1) [0.4]	37.7 (0.2) [0.1]	55.3 (0.05)	78.38 (15)	36.62 (0.9)	55.37	75.34 (16)	35.56 (4)	143 $I = 7/2$ $J = 4$
127.49 (0.002) [0.01]	88 (1) [0.1]	411.7 (1) [0.2]	127.3 (0.1)	172.86 (55)	377.14 (23)	127.3	66.29 (3)	411.43 (69)	143 $I = 7/2$ $J = 3$
135.60 (0.002) [0.01]	76 (2) [2]	57.9 (0.5) [0.3]	135.4 (0.1)	51.00 (12)	64.00 (6)	135.4	65.37 (14)	70.86 (11)	143 $I = 7/2$ $J = 3$
159.04 (0.004) [0.02]	63 (1) [0.4]	977 (4) [2]	158.7 (0.1)	175.56 (109)	924.44 (44)	159	75.56 (3)	1066.67 (107)	143 $I = 7/2$ $J = 4$
179.71 (0.003) [0.02]	76 (1) [0.2]	733 (2) [0.4]	179.5 (0.2)	142.86 (49)	657.14 (29)	179.5	86.86 (6)	731.43 (114)	143 $I = 7/2$ $J = 3$
186.80 (0.003) [0.02]	67 (1) [0.08]	1403 (3) [0.4]	186.6 (0.2)	216.67 (134)	1333.33 (89)	185.5	76.44 (3)	1511.11 (89)	143 $I = 7/2$ $J = 4$
—	—	—	226.02 (0.2)	—	$2g\Gamma_n = 0.28$ (0.1)	—	—	—	143 $I = 7/2$
306.51 (0.007) [0.06]	69 (2) [6]	773 (4) [5]	306.2 (0.3)	275.56 (106)	684.44 (36)	306.2	71.82 (4)	631.11 (124)	143 $I = 7/2$ $J = 4$
324.77 (0.008) [0.06]	70 (2) [1]	1041 (6) [3]	324.4 (0.3)	244.29 (110)	925.71 (46)	324.4	58.51 (8)	491.43 (137)	143 $I = 7/2$ $J = 3$
337.49 (0.009) [0.05]	66 (2) [0.2]	789 (7) [3]	337.1 (0.3)	100.56 (103)	684.44 (27)	337	56.53 (3)	462.22 (71)	143 $I = 7/2$ $J = 4$
350.71 (0.02) [0.05]	87 (3) [0.3]	1010 (14) [7]	350.3 (0.3)	117.14 (106)	902.86 (34)	350.3	86.17 (5)	685.71 (160)	143 $I = 7/2$ $J = 3$
401.93 (0.002) [0.07]	67 (3) [2]	1050 (21) [10]	401.3 (0.4)	240.00 (109)	960.00 (44)	401.3	71.82 (4)	924.44 (178)	143 $I = 7/2$ $J = 4$
408.49 (0.002) [0.06]	82 (3) [1]	630 (14) [21]	408 (0.4)	88.57 (69)	571.43 (34)	407.9	78.17 (4)	525.71 (91)	143 $I = 7/2$ $J = 3$
446.5 (0.001) [0.1]	82 (3) [2]	1787 (9) [4]	446.3 (0.4)	117.78 (109)	1742.22 (44)	446.1	71.47 (4)	1600 (142)	143 $I = 7/2$ $J = 4$

(Continued)

TABLE V (Continued)

RPI			Tellier			Rohr, Weigmann, and Heske			
E (eV)	Γ_γ (meV)	Γ_n (meV)	E (eV)	Γ_γ (meV)	Γ_n (meV)	E (eV)	Γ_γ (meV)	Γ_n (meV)	Isotope and Spin
^{144}Nd									
374.40 (0.002) [0.06]	108 (1) [3]	16730 (13) [18]	373.8 (0.4)	1250.0 (2062)	16250.0 (500)	—	—	—	146 $I = 0$ $J = 1/2$
^{145}Nd									
4.36 (0.0002) [0.002]	69.6 (0.4) [0.1]	1.18 (0.003) [0.003]	—	—	—	—	—	—	145 $I = 7/2$ $J = 3$
42.55 (0.0008) [0.004]	64.9 (0.4) [0.05]	372.1 (0.7) [0.08]	42.51 (0.05)	71.14 (26)	358.86 (17)	42.77	59.66 (3)	354.29 (37)	145 $I = 7/2$ $J = 3$
85.73 (0.003) [0.007]	51 (3) [4]	11.8 (0.1) [0.03]	85.61 (0.08)	66.09 (8)	11.91 (0.4)	85.61	—	9.96 (1)	145 $I = 7/2$ $J = 3$
96.15 (0.006) [0.007]	60 (12)	6.6 (0.1) [0.03]	96 (0.1)	74.06 (10)	5.94 (0.3)	96.04	—	5.71 (0.2)	145 $I = 7/2$ $J = 4$
102.08 (0.001) [0.009]	69 (1) [0.4]	133.5 (0.7) [0.2]	102.95 (0.1)	96.14 (16)	118.86 (5)	102	47.09 (4)	128.00 (9)	145 $I = 7/2$ $J = 3$
103.60 (0.002) [0.009]	66 (3) [1]	32.6 (0.3) [0.1]	103.45 (0.1)	58.38 (15)	36.62 (1)	103.4	53.87 (14)	32.00 (4)	145 $I = 7/2$ $J = 3$
147.30 (0.005) [0.01]	42 (3) [8]	21.8 (0.3) [0.5]	147.1 (0.2)	94.56 (15)	20.44 (2)	147.1	—	18.31 (1)	145 $I = 7/2$ $J = 4$
151.62 (0.009) [.01]	64 (5) [2]	13.7 (0.4) [0.3]	151.4 (0.2)	75.49 (8)	13.51 (0.4)	151.4	—	12.62 (0.7)	145 $I = 7/2$ $J = 4$
169.94 (0.03) [0.01]	60 (6) [2]	4.4 (0.2) [0.04]	169.7 (0.2)	—	2.84 (0.2)	169.6	—	2.24 (0.3)	145 $I = 7/2$ $J = 4$
189.45 (0.01) [0.01]	82 (6) [4]	36 (1) [0.4]	189.2 (0.2)	74.57 (10)	35.43 (1)	189.2	38.4 (2)	48.00 (5)	145 $I = 7/2$ $J = 4$
233.00 (0.03) [0.1]	57 (6) [3]	6.3 (0.4) [0.4]	232.6 (0.2)	93.71 (20)	7.29 (0.3)	232.6	—	5.51 (0.4)	145 $I = 7/2$ $J = 3$
242.53 (0.009) [0.03]	48 (2) [1]	62 (1) [0.7]	242.1 (0.2)	76.00 (15)	64.00 (3)	242.2	43.73 (4)	60.44 (5)	145 $I = 7/2$ $J = 4$
248.70 (0.03) [0.4]	57 (6) [2]	5.0 (0.4) [0.2]	248.4 (0.2)	—	4.57 (0.2)	248.4	—	3.64 (0.7)	145 $I = 7/2$ $J = 3$

(Continued)

TABLE V (Continued)

RPI			Tellier			Rohr, Weigmann, and Heske			
E (eV)	Γ_γ (meV)	Γ_n (meV)	E (eV)	Γ_γ (meV)	Γ_n (meV)	E (eV)	Γ_γ (meV)	Γ_n (meV)	Isotope and Spin
^{145}Nd (Continued)									
259.25 (0.008) [0.03]	55 (2) [2]	82 (1) [1]	258.9 (0.2)	78.78 (16)	86.22 (4)	258.9	38.4 (2)	99.56 (9)	145 $I = 7/2$ $J = 3$
275.19 (0.008) [0.04]	53 (2) [1]	142 (2) [2]	274.8 (0.2)	81.33 (16)	138.67 (6)	274.8	41.07 (2)	119.11 (11)	145 $I = 7/2$ $J = 4$
306.71 (0.06) [0.3]	33 (3) [2]	50 (5) [10]	—	—	—	306.2	34.74 (6)	66.29 (14)	145 $I = 7/2$ $J = 3$
311.54 (0.01) [0.05]	61 (2) [0.8]	418 (7) [4]	311.1 (0.3)	94.29 (53)	365.71 (17)	311	42.74 (3)	345.14 (34)	145 $I = 7/2$ $J = 3$
318.78 (0.03) [0.5]	61 (6) [3]	10.5 (0.8) [0.8]	318.4 (0.3)	69.51 (30)	10.49 (0.9)	318.5	—	10.84 (0.9)	145 $I = 7/2$ $J = 4$
342.89 (0.01) [0.09]	70 (6) [12]	51 (3) [1]	342.5 (0.3)	315.83 (165)	26.67 (3)	342.5	—	—	145 $I = 7/2$ $J = 4$
376.14 (0.02) [0.4]	59 (6) [2]	10 (1) [2]	—	—	—	376.6	—	9.07 (0.5)	145 $I = 7/2$ $J = 4$
390.98 (0.08) [0.07]	40 (3) [23]	50 (4) [24]	390.5 (0.4)	129.33 (50)	90.67 (4)	390.4	22.58 (3)	40.89 (7)	145 $I = 7/2$ $J = 4$
397.80 (0.1) [0.5]	74 (7) [0.5]	28 (3) [2]	397.7 (0.4)	94.14 (50)	30.86 (1)	397.8	—	—	145 $I = 7/2$ $J = 3$
404.21 (0.04) [0.07]	61 (4) [4]	230 (15) [36]	403.8 (0.4)	254.44 (53)	195.56 (18)	403.8	—	—	145 $I = 7/2$ $J = 4$
406.49 (0.05) [0.1]	50 (4) [12]	120 (9) [19]	406.2 (0.4)	—	115.56 (4)	406.1	—	—	145 $I = 7/2$ $J = 4$
446.58 (0.08) [0.1]	52 (5) [2]	150 (14) [16]	445.8 (0.4)	160.00 (35)	200.00 (17)	445.8	57.83 (4)	269.71 (30)	145 $I = 7/2$ $J = 3$
465.16 (0.02) [0.1]	82 (4) [1]	800 (10) [5]	464.4 (0.5)	211.43 (108)	748.57 (40)	464.7	58.51 (5)	706.29 (117)	145 $I = 7/2$ $J = 3$
487.59 (0.05) [0.1]	65 (4) [5]	230 (19) [15]	487.1 (0.5)	—	302.22 (13)	487.1	46.93 (3)	352.00 (27)	145 $I = 7/2$ $J = 4$
497.87 (0.02) [0.1]	68 (4) [0.06]	455 (9) [8]	497.2 (0.5)	42.86 (38)	457.14 (23)	497.2	62.86 (6)	427.43 (130)	145 $I = 7/2$ $J = 3$
(Continued)									

TABLE V (Continued)

RPI			Tellier			Rohr, Weigmann, and Heske			
E (eV)	Γ_γ (meV)	Γ_n (meV)	E (eV)	Γ_γ (meV)	Γ_n (meV)	E (eV)	Γ_γ (meV)	Γ_n (meV)	Isotope and Spin
^{146}Nd									
359.85 (0.007) [0.1]	35.23 (2) [9]	49.05 (3) [17]	359.5 (0.3)	65.5 (20)	44.5 (3)	—	—	—	146 $I = 0$ $J = 1/2$
^{148}Nd									
94.93 (0.04) [0.02]	46 (5) [2]	0.55 (0.04) [0.01]	94.9 (0.1)	—	0.27 (0.03)	—	—	—	148 $I = 0$ $J = 1/2$
155.59 (0.004) [0.02]	41.8 (0.8) [0.4]	2034 (5) [2]	155.4 (0.1)	250 (283)	1850.0 (200)	—	—	—	148 $I = 0$ $J = 1/2$
172.4 (0.1) [0.01]	45 (5) [0.2]	0.45 (0.04) [0.07]	172.4 (0.2)	—	0.41 (0.03)	—	—	—	148 $I = 0$ $J = 1/2$
184.4 (0.2) [0.08]	45 (5) [0.02]	0.071 (0.007) [0.001]	184.5 (0.2)	—	0.67 (0.03)	—	—	—	148 $I = 0$ $J = 1/2$
252.9 (0.2) [0.4]	45 (5) [0.1]	0.38 (0.004) [0.02]	252.9 (0.2)	—	0.40 (0.08)	—	—	—	148 $I = 0$ $J = 1/2$
287.66 (0.006) [0.04]	35 (1) [0.2]	3043 (6) [3]	287.5 (0.3)	50 (224)	3130.00 (100)	—	—	—	148 $I = 0$ $J = 1/2$
398.84 (0.03) [0.08]	59 (3) [3]	340 (14) [7]	398.3 (0.4)	—	350.00 (30)	—	—	—	148 $I = 0$ $J = 1/2$
^{150}Nd									
78.92 (0.002) [0.007]	45 (2) [6]	17.3 (0.1) [0.1]	78.82 (0.07)	52.1 (10)	18.90 (0.5)	—	—	—	150 $I = 0$ $J = 1/2$
265.9 (0.3) [0.06]	52 (5) [0.01]	0.39 (0.04) [0.02]	265.9 (0.2)	—	0.40 (0.05)	—	—	—	150 $I = 0$ $J = 1/2$
313.62 (0.01) [0.05]	55 (2) [1]	402 (6) [4]	313.2 (0.3)	85 (52)	425.00 (15)	—	—	—	150 $I = 0$ $J = 1/2$
458.9 (0.1) [0.6]	52 (5) [0.1]	1.5 (0.1) [0.02]	459 (0.5)	—	1.50 (0.3)	—	—	—	150 $I = 0$ $J = 1/2$
486.4 (0.02) [0.1]	56 (3) [3]	1030 (18) [9]	486 (0.5)	145 (112)	975.00 (50)	—	—	—	150 $I = 0$ $J = 1/2$

*The RPI parameters have errors from SAMMY fits in parentheses ( ) and errors from the resolution function in square brackets [ ]. The errors from Tellier and Rohr, Weigmann, and Heske are presented in parentheses.

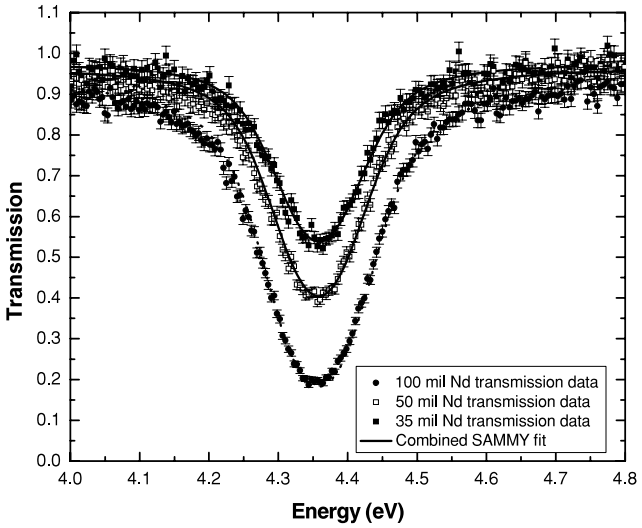

Fig. 1. Combined SAMMY fit with final RPI neodymium parameters for transmission in the energy region of 4.0 to 4.8 eV.

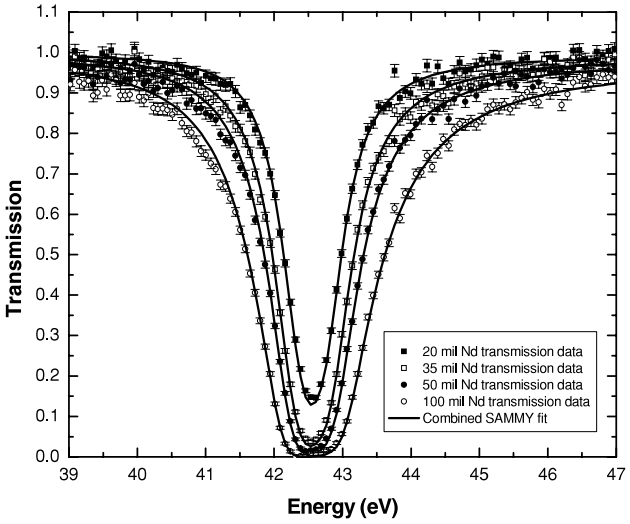

Fig. 3. Combined SAMMY fit with final RPI neodymium parameters for transmission in the energy region of 39 to 47 eV.

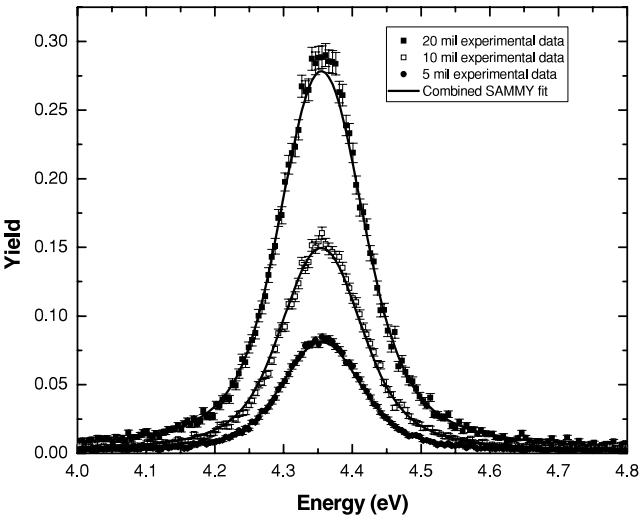

Fig. 2. Combined SAMMY fit with final RPI neodymium parameters for yield in the energy region of 4.0 to 4.8 eV.

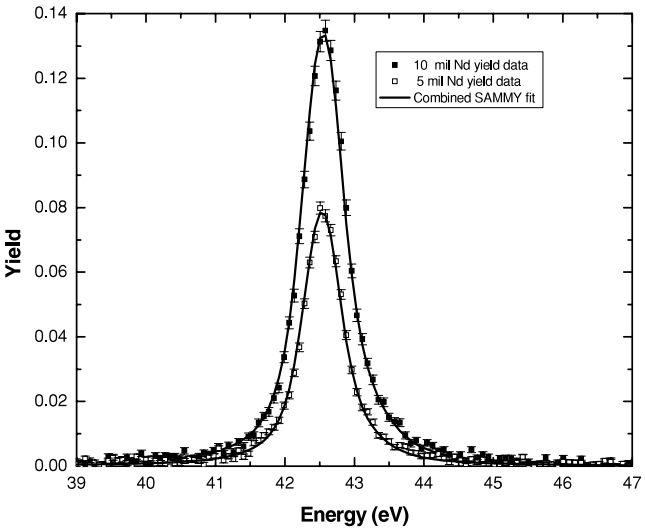

Fig. 4. Combined SAMMY fit with final RPI neodymium parameters for yield in the energy region of 39 to 47 eV.

Tellier parameters were fixed to the ENDF/B-VI spin values, permitting the calculation of Γ_n and Γ_γ. In those cases in which no information was provided about Γ_γ, its value was deduced by taking the difference $\Gamma_t - \Gamma_n$. As a result of this procedure, it is readily apparent that the Tellier resonance parameters show large fluctuations in Γ_γ. The Rohr, Weigmann, and Heske parameters were given in terms of $g\Gamma_n$ and $g\Gamma_\gamma$. Once again, any unknown spins were fixed to the ENDF/B-VI values in order to determine Γ_n and Γ_γ. The Rohr, Weigmann, and Heske values of Γ_γ seemed to make more sense in that they did not vary much.

When the RPI parameters for neodymium are compared to the previously published parameters in Tables IV and V, a few things can be noticed. The energy for each resonance changes very little when compared with the energy values quoted from the other sources. Most of the RPI values of Γ_n for each neodymium isotope are larger than those previously published. The smaller values of Γ_n previously published may be the result of inaccurate treatment of Doppler broadening or the resolution function. The biggest differences in Γ_n arise within the energy range of 300 and 500 eV. This may be due to the effect of the massive ^{144}Nd scattering resonance found at

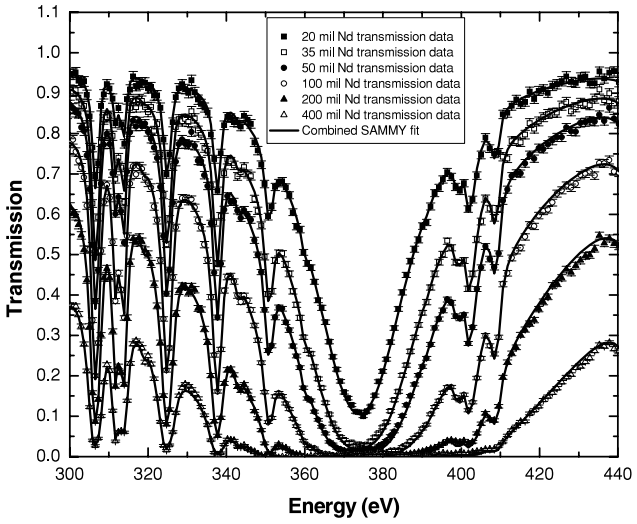

Fig. 5. Combined SAMMY fit with final RPI neodymium parameters for transmission in the energy region of 300 to 440 eV.

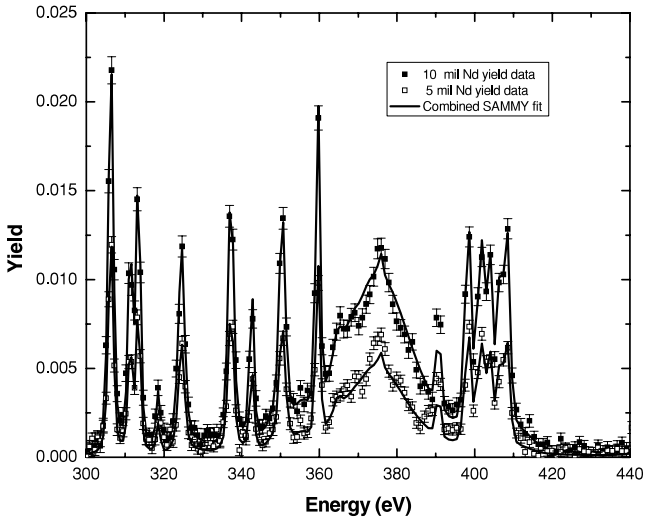

Fig. 6. Combined SAMMY fit with final RPI neodymium parameters for yield in the energy region of 300 to 440 eV.

374.4 eV. The RPI Γ_γ parameters behave as expected from theory since they do not vary much within each isotope. The RPI values of Γ_γ are comparable to those previously published, with the exception of the Tellier parameters. It is apparent that the overall errors on the RPI neodymium resonance parameters are less than those quoted for the previously published parameters. This can be explained by that fact that the RPI data are a result of high-quality measurements that were performed to ensure good counting statistics, which led to small statistical errors. Additionally, the fitting errors from SAMMY and the systematic errors introduced by the resolution function were also small.

The average radiation width for each neodymium isotope is presented in Table VI. All of the average values and errors in Table VI were found by using a weighted average technique. The only exceptions were for the ^{144}Nd and ^{146}Nd isotopes, each of which had only one known resonance. In such instances a weighted average could not be taken, and the value of the RPI radiation width in Table IV was used. These one-point values of the radiation width are listed in Table VI within parentheses.

The resonance integral (RI) was calculated for each neodymium isotope using the NJOY code[14] and INTER code.[15] The NJOY code was used to reconstruct room-temperature pointwise cross sections given either the ENDF/B-VI or the final RPI neodymium resonance parameters, while the INTER code was used to perform the integration under this cross section to calculate the resonance integral. The resonance integral RI may be defined mathematically[16] as follows:

$$RI = \int_{E_{min}}^{E_{max}} \sigma_C(E)\,\frac{dE}{E} \quad , \tag{3}$$

where $\sigma_C(E)$ is the capture cross section in barns generated by NJOY with neodymium resonance parameters and E is the energy in electron volts. The resonance integrals were calculated for both the RPI and ENDF/B-VI parameters within the energy region of 1 to 500 eV. The results are presented in Table VII for all naturally occurring neodymium isotopes. It should be noted that the ^{142}Nd isotope has no known resonances in this energy region; therefore, the capture resonance integral calculated from the ENDF/B-VI parameters for ^{142}Nd was assumed to be correct. The capture resonance integral changes very little for ^{143}Nd, while all other capture resonance integrals did change with respect to ENDF/B-VI. The most noticeable change was observed in the

TABLE VI

Average Radiation Width for Each Neodymium Isotope in the Energy Range from 1 to 1000 eV*

Neodymium Isotope	Average Radiation Width $\langle\Gamma_\gamma\rangle$ (meV)
143	72 ± 1
144	(108 ± 3)
145	66 ± 1
146	(35 ± 9)
148	45 ± 1
150	55 ± 1

*The parentheses denote an isotope for which only one resonance was available.

TABLE VII

Calculated Capture Resonance Integrals for RPI and ENDF/B-VI Parameters, Respectively*

Neodymium Isotope	Abundance, f_i	Capture Resonance Integrals from Resonances in the Energy Range 1 to 500 eV	
		RPI (b)	ENDF (b)
142	0.2713	(5.834)	5.834
143	0.1218	89.5 ± 0.2	89.51
144	0.238	4.5 ± 0.1	3.47
145	0.083	206.8 ± 0.5	227.74
146	0.1719	1.08 ± 0.1	1.21
148	0.0576	11.0 ± 0.2	16.97
150	0.0564	11.69 ± 0.02	13.10
Natural neodymium	$\Sigma RI_i f_i$	32 ± 1	34.14

*The integrations were performed over the energy region from 1 to 500 eV. The parentheses ( ) signify that the capture resonance integral was kept the same as the ENDF value.

^{145}Nd capture resonance integral, which decreased significantly with the RPI parameters. This change in the capture resonance integral is directly attributed to the changes in the 4.36-eV resonance parameters. The capture resonance integral for natural neodymium isotopes was calculated to be 32 ± 1 b. This is slightly lower than the ENDF/B-VI capture resonance value of 34.14 b. A method was developed to estimate the errors of each of the resonance integral calculations. This method was formulated by taking partial derivatives of the single-level Breit-Wigner equation[16] for the capture cross section using the Mathcad program[17] and propagating the errors in the resonance parameters to the resonance integral.

VI. CONCLUSIONS

The values of the RPI neodymium resonance energies change very little when compared to the previously published parameters. A majority of the RPI values for the neutron width Γ_n are larger than those published previously. A noticeable exception is the resonance found at 4.36 eV for which the Γ_n found is lower than previously published. The smaller values quoted previously may be due to inaccurate treatment of Doppler broadening or resolution function shape. The RPI values of Γ_γ are comparable to those previously published, with the exception of the Tellier parameters, which varied greatly. The overall errors on the RPI neodymium parameters are less than those quoted in the previously published parameters. These small errors are attributed to the high-quality RPI measurements that were performed to ensure good counting statistics, which led to small statistical errors. Additionally, the fitting errors from SAMMY and the systematic errors introduced by the resolution function were also small. The resulting resonance parameters were used to calculate the capture resonance integral with this energy region and were compared to calculations obtained when using the resonance parameters from ENDF/B-VI. The RPI parameters gave a resonance integral value of 32 ± 1 b, which is ~2.14 b (~7%) lower than that obtained with the ENDF/B-VI parameters. The decrease in the RPI capture resonance integral with respect to ENDF/B-VI is directly attributed to the decrease in the Γ_n value for the 4.36-eV neodymium resonance.

REFERENCES

1. N. M. LARSON, "Updated Users Guide for SAMMY: Multilevel R-Matrix Fits to Neutron Data Using Bayes' Equations," ORNL/TM-9179/R5, Lockheed Martin Energy Research Corporations, Oak Ridge National Laboratory (2000).

2. R. C. BLOCK, P. J. MARANO, N. J. DRINDAK, F. FEINER, K. J. SEEMANN, and R. E. SLOVACEK, "A Multiplicity Detector for Accurate Low-Energy Neutron Capture Measurements," *Proc. Int. Conf. Nuclear Data for Science and Technology*, Mito, Japan, May 30–June 3, 1988, p. 383.

3. R. E. SLOVACEK, R. C. BLOCK, Y. DANON, C. WERNER, G. U. YOUK, J. A. BURKE, N. J. DRINDAK, F. FEINER, J. A. HELM, and K. W. SEEMANN, "Neutron Cross-Section Measurements at the Rensselaer LINAC," *Proc. Topl. Mtg. Advances in Reactor Physics*, Knoxville, Tennessee, April 11–15, 1994, Vol. II, p. 193, American Nuclear Society (1994).

4. M. E. OVERBERG, B. E. MORETTI, R. E. SLOVACEK, and R. C. BLOCK, "Photoneutron Target Development for the

RPI Linear Accelerator," *Nucl. Instrum. Methods Phys. Res. A*, **438**, 253 (1999).

5. Y. DANON, R. E. SLOVACEK, and R. C. BLOCK, "The Enhanced Thermal Neutron Target at the RPI LINAC," *Trans. Am. Nucl. Soc.*, **68**, 473 (1993).

6. Y. DANON, R. E. SLOVACEK, and R. C. BLOCK, "Design and Construction of a Thermal Neutron Target for the RPI LINAC," *Nucl. Instrum. Methods Phys. Res. A*, **352**, 596 (1995).

7. D. P. BARRY, "Neodymium Neutron Transmission and Capture Measurements and Development of a New Transmission Detector," Doctoral Thesis, Rensselaer Polytechnic Institute (2003).

8. D. B. SYME, "The Black and White-Filter Method for Background Determination in Neutron Time-of-Flight Spectrometry," *Nucl. Instrum. Methods*, **198**, 357 (1982).

9. CROSS SECTION EVALUATION WORKING GROUP, "ENDF/B-VI Summary Documentation," BNL-NCS-17541 (ENDF-201), P. R. ROSE, Ed., National Nuclear Data Center, Brookhaven National Laboratory (1991).

10. S. F. MUGHABGHAB, M. DIVADEENAM, and N. E. HOLDEN, *Neutron Cross Sections*, Academic Press, New York and London (1984).

11. H. TELLIER, "Properties of Levels Induced by Resonance Neutrons in Stable Neodymium Isotopes," CEA-N-1459, Commissariat à l'Energie Atomique (1971).

12. H. TELLIER, *C. R. Acad. Sc. Paris Ser. B*, **272**, 695 (1971).

13. G. ROHR, H. WEIGMANN, and M. HESKE, "Neutron Capture and γ-Ray Spectra Measurements in Resolved Resonances for the Odd Nd Isotopes," *Proc. Conf. Neutron Cross Sections and Technology*, Knoxville, Tennessee, March 1971, p. 743 (1971).

14. R. E. MacFARLANE and D. W. MUIR, "The NJOY Nuclear Data Processing System Version 91," LA-12740-M, Los Alamos National Laboratory (Oct. 1994).

15. C. L. DUNFORD, "ENDF Utility Codes Release 6.12," Informal Report (Apr. 2001).

16. J. J. DUDERSTADT and L. J. HAMILTON, *Nuclear Reactor Analysis*, Wiley and Sons, New York (1976).

17. MATHCAD, Version 2000, Professional, MathSoft, Inc.